2003

A Mathematical Model of Oxide/Carbon Composite Electrode for Supercapacitors

Hansung Kim
University of South Carolina - Columbia

Branko N. Popov
University of South Carolina - Columbia, popov@engr.sc.edu

Publication Info

Journal of the Electrochemical Society, 2003, pages A1153-A1160.

Publisher's link: http://dx.doi.org/10.1149/1.1593039
DOI: 10.1149/1.1593039

Journal of The Electrochemical Society, **150** (9) A1153-A1160 (2003)
0013-4651/2003/150(9)/A1153/8/$7.00 © The Electrochemical Society, Inc.

A Mathematical Model of Oxide/Carbon Composite Electrode for Supercapacitors

Hansung Kim* and Branko N. Popov,z**

Center for Electrochemical Engineering, Department of Chemical Engineering, University of South Carolina, Columbia, South Carolina 29208, USA

A pseudo two-dimensional model is developed for the general application of supercapacitors consisting of an oxide/carbon composite electrode. The model takes into account the diffusion of protons in the oxide particle by employing the method of superposition. RuO_2/carbon system is modeled as a specific example. From the simulation data, it is found that the oxide particle size and proton diffusion coefficient have an enormous effect on the performance at high discharge rate due to the limitation of proton transport into RuO_2 particles. With increasing carbon ratio, the porosity of electrode increases, which causes the potential drop in solution phase to decrease. However, excess of carbon lowers the total capacitance because the pseudocapacitance from RuO_2 decreases. Finally, the present model successfully provides a methodology to optimize cell configurations and operating conditions.
 [DOI: 10.1149/1.1593039]

Manuscript submitted September 3, 2002; revised manuscript received March 8, 2003. Available electronically July 10, 2003.

Supercapacitors can be divided into two categories: electric double-layer capacitors and pseudocapacitors. Electric double-layer capacitors exhibit capacitance due to charge separation between a solid electrode and an electrolyte. In contrast, pseudocapacitance results from the chemisorption of active ion or the faradaic redox reaction occurring on the transition metal oxide.

For the double-layer capacitors, various mathematical models have been developed to analyze their performance. Posey and Morozumi[1] developed macroscopic equations to explain the behavior of double-layer capacitors under potentiostatic and galvanostatic charging in porous electrodes. Johnson and Newman[2] developed a model to describe double-layer charging in an electrochemical cell and to predict the specific energy and power densities of electrochemical capacitors. Pillay and Newman[3] modeled the influence of side reactions on the performance of electrochemical capacitors. Srinivasan and Weidner[4] presented an analytical solution of the double-layer capacitor under constant current mode, which was used to investigate the relative importance of ionic and electronic resistance in the design of supercapacitors. Farahmandi[5] also presented an analytic solution of the model for double-layer capacitors to study the effects of both ionic and solid-phase conductivities on the behavior of an electrochemical capacitor.

Few models have been developed for pseudocapacitance. Lin *et al.*[6] reported a supercapacitor model, which considers the faradaic reaction occurring on RuO_2. It was modified to include both double-layer capacitance and pseudocapacitance using the packing theory and the concentrated solution theory.[7] This model explained the effect of the particle size of the oxide and of the cell current density on the charge/discharge behavior. However, this model did not analyze the difference in capacitance exhibited by crystalline and amorphous RuO_2. It is well known in literature[8,9] that proton transfer rates within ruthenium oxide particle determines the capacitance of the electrode. An amorphous structure allows the proton to diffuse faster inside the oxide particle as compared to crystalline RuO_2. The proton transfer rate and the capacitance obtained are related closely and strongly depend on the degree of crystallinity of the Ru oxide. The model by Lin *et al.*[6] does not consider proton diffusion and hence cannot distinguish between different forms of ruthenium oxide. As a result, this model has limitations when applied to the real system. To overcome this problem, in this paper we consider the proton diffusion in oxide particles using the procedure presented by Doyle *et al.*[10] The present model successfully provides a theoretical simulation of the charge or discharge behavior of a hybrid supercapacitor as a function of cell parameters such as the porosity of electrode, the particle size of oxide, the concentration of electrolyte, and the ratio between oxide and carbon.

The objective of this study is to develop a general full cell model for supercapacitors which considers the diffusion of protons within the oxide particle. The goal is to develop a model which considers both the pseudocapacitance and double-layer capacitance. Using this model, the effect of particle size, porosity, and the ratio of active material in the electrode on capacitor performance is evaluated.

Model

Figure 1 shows a schematic diagram of a typical supercapacitor cell. It consists of two identical RuO_2/carbon composite electrodes and an ionically conductive separator. A solution of H_2SO_4 used as the electrolyte fills the pores completely in the electrodes and the separator. The system was simulated along the x direction assuming that at each point the faradaic redox reactions occur on the surface of the RuO_2 particles during charge/discharge as follows[11]

$$H_{0.8+\delta}RuO_2 \leftrightarrow H_{0.8}RuO_2 + \delta H^+ + \delta e^- \qquad [1]$$

A process of diffusion of oxidation state involving proton and electron hopping refreshes the surface of RuO_2.[12] As a result, it can be considered that the transport of protons takes place in the bulk of RuO_2 particles, therefore making this a pseudo two-dimensional (2D) problem.

The present model was developed with the following assumptions. The diffusion coefficient in the solid and solution phase is independent of electrolyte concentration. The entire surface contributes to the double-layer capacitance. The double-layer capacitance per area (P_d) is constant. The exchange current density, transference number, and activity coefficient are not a function of the concentration of electrolyte. Also all side reaction and temperature effects are neglected. Further, both electrodes have the same thickness.

In this model, there are four variables: C (concentration of electrolyte), Φ_1 (potential in the solid phase), Φ_2 (potential in the solution phase), C_s (concentration of proton in the oxide particle). Therefore, all governing equations were converted to the forms containing only these variables using the conservation of charge and Ohm's law in the solid phase. These are represented as

$$I = i_1 + i_2, \quad 0 = \frac{\partial i_1}{\partial x} + \frac{\partial i_2}{\partial x} \qquad [2]$$

$$i_1 = -\sigma \frac{\partial \Phi_1}{\partial x} \qquad [3]$$

* Electrochemical Society Student Member.
** Electrochemical Society Active Member.
z E-mail: popov@engr.sc.edu

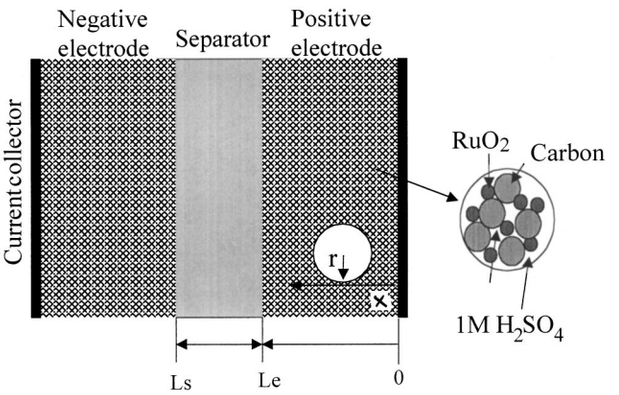

Figure 1. Schematic diagram of supercapacitor upon which the model is based.

where i_1 and i_2 are the superficial current density in the solid and solution phase, respectively, while σ is the electronic conductivity in the solid phase. In the previous model,[6,7] the total current transferred from the solid phase to the electrolyte phase was expressed by the sum of two contributions: the double-layer charge and the faradaic redox reaction. These two contributions are defined as follows

$$\frac{\partial i_2}{\partial x} = \sigma \frac{\partial^2 \Phi_1}{\partial x^2} = S_d P_d \frac{\partial(\Phi_1 - \Phi_2)}{\partial t} + S_f j_f \qquad [4]$$

$$S_d = S_c + S_f = A_C \rho_C v_C (1 - \varepsilon) + \frac{6 v_{RuO_2}(1 - \varepsilon)}{d_{RuO_2}} \qquad [5]$$

where S_d represents the specific surface area for double-layer capacitance per unit volume, ε is the porosity in the electrode, and A_c is the specific surface area of carbon. S_f represents the specific surface area for pseudocapacitance per unit electrode volume, while v_c and ρ_c are volume fraction of carbon and density of carbon, respectively. Because we assume that the entire surface contributes to the double-layer charge, it can be described by the sum of S_c from carbon and S_f from RuO_2.

In Eq. 4, j_f is the faradaic transfer current density for the RuO_2 redox reaction. Using Butler-Volmer equation, it has a kinetic expression of the form

$$j_f = i_0\{\exp[\alpha_a(\Phi_1 - \Phi_2 - U_1)F/RT] - \exp[-\alpha_c(\Phi_1 - \Phi_2 - U_1)F/RT] \qquad [6]$$

where U_1 is the equilibrium potential for the electrode reaction. According to the experimental data reported, the equilibrium potential varies linearly as a function of hydrogen content.[11] The potential of the RuO_2 electrode [*vs.* saturated calomel electrode (SCE)] is 0.0 V for a hydrogen content of 1.3 and 1.0 V for 0.3, and 0.5 V for 0.8. From this relationship, U_1 is defined by

$$U_1 = 2V_0\left(- \frac{M_{RuO_2}}{\rho_{RuO_2}} C_s + 1.3 \right) \qquad [7]$$

where V_0 is the initial equilibrium potential before charging, taken as 0.5 V.

A material balance on the electrolyte can be expressed as follows using concentrated solution theory[13] and by assuming a binary electrolyte

$$\varepsilon \frac{\partial C}{\partial t} = \nabla \cdot \left(\varepsilon D(C)\left(1 - \frac{d(\ln C_0)}{d(\ln C)}\right)\nabla C \right) - \frac{i_2 \cdot \nabla t_+^0(C)}{z^+ v^+ F} \qquad [8]$$

where C is the concentration of the electrolyte. In the separator region, this equation can be simplified based on the assumptions listed previously to

$$\frac{\partial C}{\partial t} = D \frac{\partial^2 C}{\partial x} \qquad [9]$$

Similarly, a material balance on the electrolyte in the porous electrode is given by

$$\varepsilon \frac{\partial C}{\partial t} = \varepsilon D \frac{\partial^2 C}{\partial x^2} - \frac{s_i}{nF} \sigma \frac{\partial^2 \Phi_1}{\partial x^2} \frac{(1 - t_+^0)}{v^+} \qquad [10]$$

The extra term compared to the above equation accounts for the reaction term taking place in the electrode. The current distribution in the porous electrode is calculated from[14]

$$i_2 = I - i_1 = I + \sigma \frac{\partial \Phi_1}{\partial x} = -\kappa_P \frac{\partial \Phi_2}{\partial x} - \frac{\kappa_P RT}{F}\left(\frac{s^+}{nv^+} + \frac{t_+^0}{z^+ v^+} \right) \frac{\partial(\ln C)}{\partial x} \qquad [11]$$

where κ_P is the ionic conductivity of the electrolyte. The same expression can be applied to the separator section. However, the electric conductivity of the separator is zero and hence the current here is carried only by the solution phase. Thus, the total current density, I, is the same as i_2.

The boundary conditions of the system include

At $x = 0$

$$\frac{\partial C}{\partial x} = 0, \quad I_{cell} = i_1 = -\sigma \frac{\partial \Phi_1}{\partial x}, \quad \frac{\partial \Phi_2}{\partial x} = 0 \qquad [12]$$

At $x = L_e = L_e + L_s$

$$\varepsilon_s^{1.5} D_0 \frac{\partial C}{\partial x_{sep}} = \varepsilon^{1.5} D_0 \frac{\partial C}{\partial x_{elec}}, \quad \frac{\partial \Phi_1}{\partial x} = 0$$

$$\varepsilon_s^{1.5} k_{po} \frac{\partial \Phi_2}{\partial x_{sep}} = \varepsilon^{1.5} k_{p0} \frac{\partial \Phi_2}{\partial x_{elec}} \qquad [13]$$

At $x = 2L_e + L_s$

$$\frac{\partial C}{\partial x} = 0, \quad I_{cell} = i_1 = -\sigma \frac{\partial \Phi_1}{\partial x}, \quad \Phi_2 = 0 \qquad [14]$$

In the above equations, the continuity concept is applied at the interface between the electrode and the separator. The diffusion coefficient of electrolyte and ionic conductivity of solution are modified from the bulk characteristics by considering the porosity of the electrode[13]

$$D = D_0 \varepsilon^{0.5}, \quad k_p = k_{p0} \varepsilon^{1.5} \qquad [15]$$

The initial conditions are

At $t = 0$

$$C = C^0, \quad \Phi_{1\,positive} = 1.0\ V, \quad \Phi_{1\,negative} = 0.0\ V \qquad [16]$$

where C^0 is the initial concentration of the electrolyte. Positive and negative electrodes are fully charged and discharged resulting in a cell potential of 1.0 V.

The diffusion in oxide particles, not considered previously, is considered here. If RuO_2 is a spherical particle of radius R_s, a material balance in the radial direction, r, is given by

$$\frac{\partial C_s}{\partial t} = D_s\left[\frac{\partial^2 C_s}{\partial r^2} + \frac{2}{r} \frac{\partial C_s}{\partial r} \right] \qquad [17]$$

Table I. Model parameters used in the simulation.

Parameter	Value	Reference
D_0	1.8×10^{-5} cm^2/s	24
Le	100 μm	Assumed
Ls	25 μm	Assumed
k_{p0}	0.8 S/cm	21
t_+^0	0.814	24
i_0	10^{-5} A/cm^2	Assumed
σ	1.0×10^3 S/cm	23
D_s	1.0×10^{-11} cm^2/s	12
ε_s	0.7	Assumed
ρ_c	0.9 g/cm^3	Assumed
ρ_{RuO_2}	2.5 g/cm^3	9
C_d	2.0×10^{-5} F/cm^2	22
C^0	1 M	Assumed
A_c	250 m^2/g	Measured

where D_s is the diffusion coefficient of proton in the oxide particle. No proton transport occurs within the carbon particles.

At the center of the particle symmetry yields

At $r = 0$

$$\frac{\partial C_s}{\partial r} = 0 \qquad [18]$$

For the other boundary condition, the rate of diffusion of proton into the surface of the oxide is related to the faradaic current produced at the particle-electrolyte interface

At $r = R_s$

$$\frac{\partial C_s}{\partial r} = -\frac{j_f}{D_s F} \qquad [19]$$

As shown before, j_f is a function of Φ_1, Φ_2, and U_1. Also, U_1 depends on C_s which in turn is related to the above governing equation. Consequently, all the variables have an influence on each other and hence they should be solved simultaneously. Because the proton concentration in the particle and the rest of the variables are related only through the time-dependent boundary condition (Eq. 19), the method of superposition was employed to simplify the calculation. This process helps in reducing the computation time. The solution can be obtained by simply summing up the solutions from all past unit step changes in concentration at the oxide surface.[10] The equations specified for the system are solved numerically using DASPK nonlinear solver[15] using the system parameters listed in Table I.

Results and Discussion

The primary objective of the present model is to study the effect of proton diffusion in the particle on the capacitor performance. Prior to doing this it is essential to fix all electrode design parameters including electrode porosity. The electrode porosity varies with the type and amount of carbon used because carbon is more porous than RuO_2. In a hybrid capacitor, the electrode porosity varies as a function of C/RuO_2 ratio. Figure 2 shows the dependence of porosity with respect to C/RuO_2 ratio in the electrode. In a previous model,[7] packing theory[16,17] was used to account for the porosity of the hybrid electrode as a function of carbon/RuO_2 ratio. The model considers only the change of free volume between different sizes of oxide particle by assuming that particles have no pores inside. As a result, the porosity of the electrode increases with RuO_2 content. However, this result conflicts with experimental observations.[18] To reflect the true porosity of the electrode, the pore volume and density were measured for both carbon and RuO_2 electrodes. Based on this data, the density and void volume of the composite electrode were calculated using the mixing rule. Finally, the porosity of the electrode was determined by dividing the void volume of the composite electrode with the total volume derived from the density of the composite electrode. As shown in Fig. 2, the porosity increased continuously with increasing the carbon ratio in the electrode. Further simulations in the paper have been done by calculating the electrode porosity based on the carbon/RuO_2 ratio.

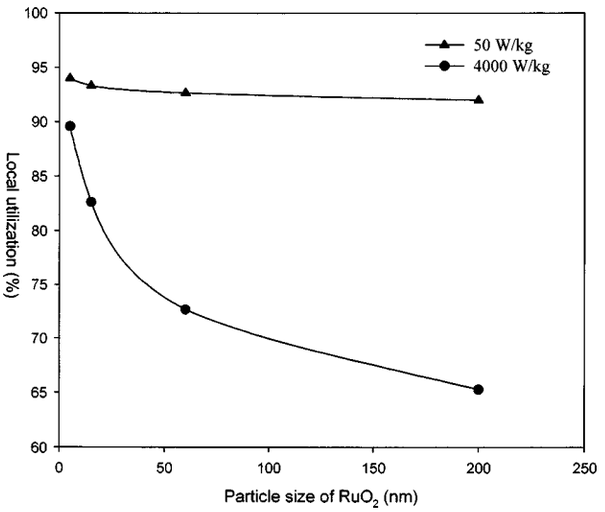

Figure 2. Porosity of the electrode as a function of RuO_2 weight fraction.

We first simulate the effect of proton transport rates in the particle on the discharge time of the capacitor. Hence the parameter of interest is the diffusion coefficient of proton in the oxide particle. We fix the discharge current (galvanostatic conditions) and simulate the change in cell potential as a function of time. Figure 3 presents the cell potential *vs.* time data for two different diffusion coefficients. Holding the discharge current constant, for both values of diffusion coefficients, a linear decay of the cell potential with time is seen. This behavior is characteristic of all capacitors. The product of the discharge current and the final discharge time divided by the cell

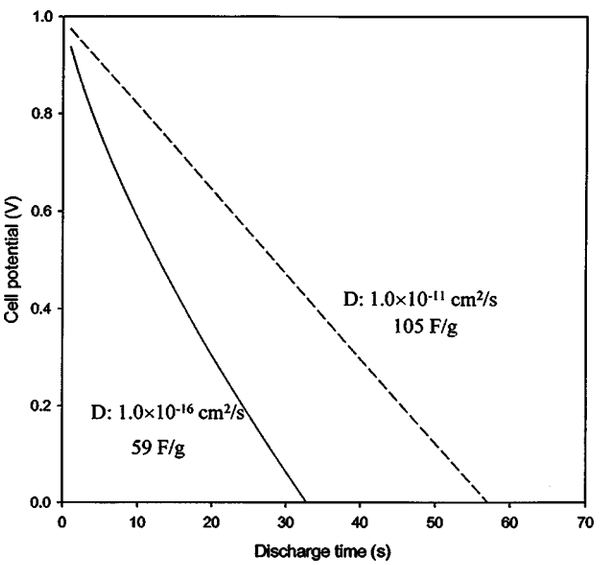

Figure 3. Effect of proton diffusion coefficient on the cell potential during a constant current discharge of 30 mA/cm^2. RuO_2: 40 wt %, porosity: 0.214, particle size: 5 nm.

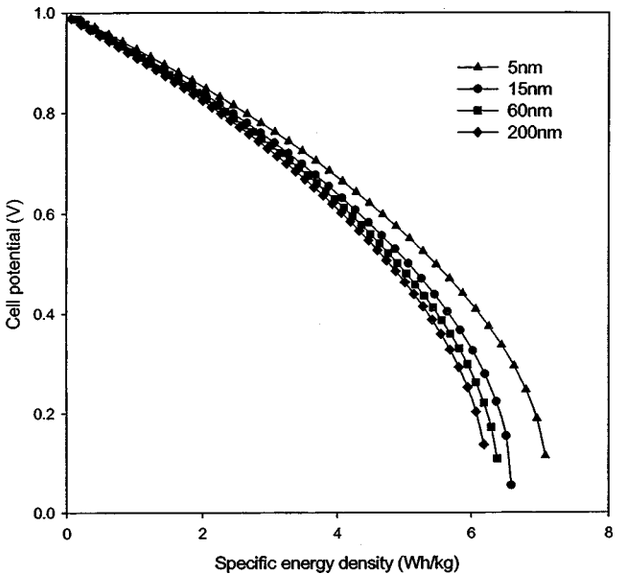

Figure 4. Specific energy density curves at a constant power discharge of 50 W/kg for different particle sizes of RuO_2. RuO_2: 40 wt %, porosity: 0.214.

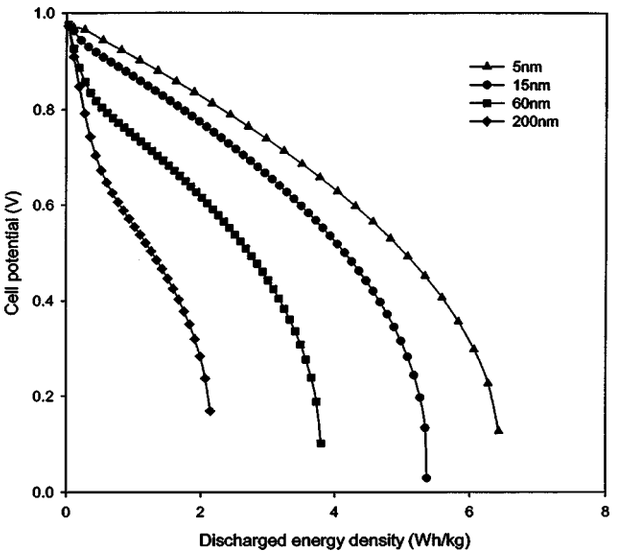

Figure 5. Specific energy density curves at a constant power discharge of 4 kW/kg for different particle sizes of RuO_2.

potential yields the capacitance of the cell. In the plot the capacitance values have been normalized to the weight of the cell which remains the same for both D values.

Because the present model accounts for the diffusion of proton in the oxide particles, a large difference in the specific capacitance is seen when changing the diffusion coefficient. When the diffusion coefficient is chosen as 10^{-11} cm^2/s,[12] the specific capacitance obtained is 105 F/g. This value corresponds to 420 F/g for a single electrode. This agrees favorably with the specific capacitance of 407 F/g measured experimentally from the single-electrode studies under similar conditions.[19] In contrast, the diffusion coefficient of 10^{-16} cm^2/s yields a capacitance of 59 F/g only. At low values of the diffusion coefficient, only protons close to the surface of the oxide particle take part in the reaction. Protons within the bulk of the RuO_2 particle are not utilized. This result clearly demonstrates the importance of proton transport rates in the oxide particle in achieving a high capacitance. According to previous studies, it is known that the diffusion coefficient of proton in the oxide is strongly dependent on factors such as oxide annealing temperature, hydration number, and the degree of crystallinity.[9,20]

For practical conditions the parameter of interest is the specific energy density of the supercapacitor. Usually this value is determined under a constant load where the specific power obtained from the device is held constant. The specific power is calculated by multiplying the discharge current with the cell potential and normalizing the product with the cell weight. Unlike batteries, supercapacitors do not exhibit a constant potential when a discharge current is applied. As shown in Fig. 3 the cell potential decreases linearly with time and hence the specific power also decreases continuously. To maintain a constant power discharge it becomes essential to increase the discharge current so that the product of current and potential remains constant. We next simulate the behavior of the cell under constant power conditions. Figure 4 and 5 demonstrate the change of energy density under the constant power discharge of 50 W/kg and 4 kW/kg, respectively. In both cases the particle size is changed from 5 to 200 nm and the proton diffusion coefficient is held constant at 1×10^{-11} cm^2/s. The simulations were run by holding the current constant. On solving for all the variables, the cell potential is determined. If this value has decreased below the preset value, the discharge current is changed and the simulations are run again. Each point in Fig. 4 and 5 have been obtained through such an iterative process. At the low discharge rate of 50 W/kg (shown in Fig. 4) the specific energy density of the electrode with 5 nm particles is about 20% higher than that of the electrode with 200 nm particles. However, particle sizes between 60 and 200 nm show similar performance, indicating that increasing particle size has little effect on the performance. This simulation result is supported by the literature data reporting that the capacitance is insensitive to the change of specific surface area of RuO_2.[9] This can be attributed to the proton transport rates in the oxide particle. Where the discharge rate is low, the discharge time is long enough for protons to diffuse and reach the core of particle. Therefore, when the reaction happens, it does not appear that the particle size has a significant effect on the performance of supercapacitors. However, at high discharge rates like 4 kW/kg (presented in Fig. 5), a different trend can be observed. With increasing particle size, the discharge energy density falls tremendously and a sharp drop in potential at the start of discharge, which is associated with faradaic kinetic resistance, is observed. This can be explained clearly by examining the local utilization of the active material between separator and electrode as shown in Fig. 6. The term ''local utilization'' refers to the amount of protons taking part in the reaction. Utilization values close to 100% indicate that all protons with the oxide particle take part in the reaction. The position at $x = L_e$ has the highest utilization in the cell because the active material in contact with the separator begins to fill up as soon as discharge begins. In 50 W/kg of discharge rate the utilization of active material does not change significantly with increasing particle size. However, at a discharge rate of 4 kW/kg, utilization decreases significantly from 90 to 65% when the particle size changes from 5 to 200 nm. Consequently, smaller particles optimize the performance of the active materials because of diffusion limitations which exist in the oxide particle.

We can also analyze the effect of particle size from the dimensionless parameter, *Sc*, which is the ratio of diffusion time in oxide particle to the discharge time for a given discharge rate[10]

$$Sc = \frac{R_s^2 I}{D_s F(1 - \varepsilon) C_t L_e} \qquad [20]$$

If this parameter is much smaller than unity, then we expect that the effect of diffusion in the oxide particle can be neglected. As shown in Fig. 7, substitution of the given parameters into Eq. 20 generates a *Sc* that is much smaller than unity over the entire range of current densities when the particle size is smaller than 15 nm. As the particle size increases, *Sc* also increases indicating that the diffusion in

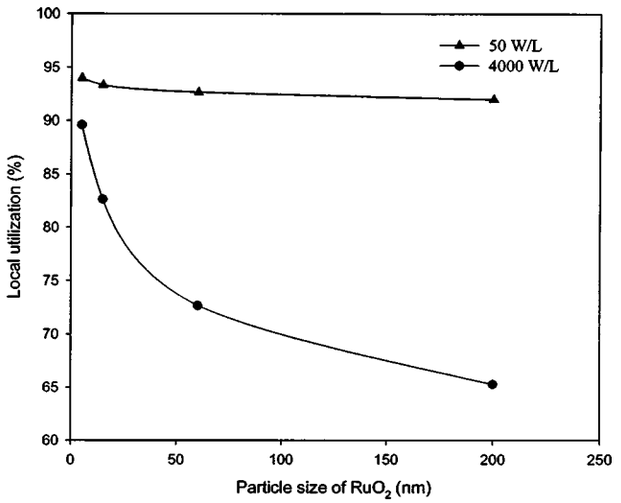

Figure 6. Local utilization of RuO_2 at the positive electrode-separator interface as a function of particle size at different discharge rates.

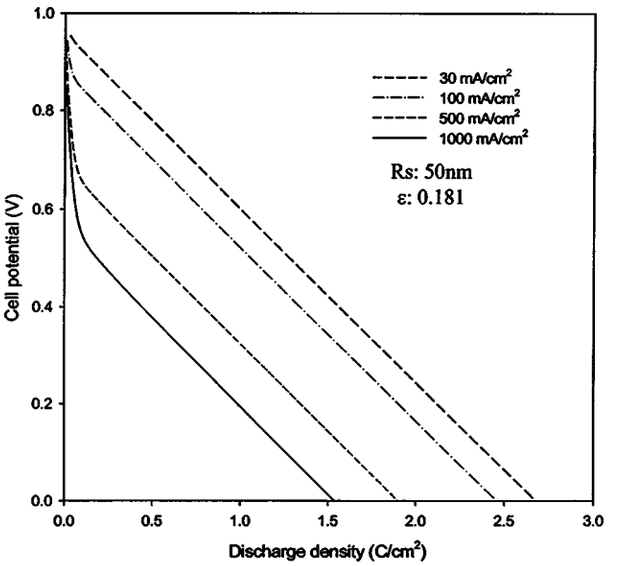

Figure 8. Electrochemical performance of the RuO_2/carbon composite electrode (60 wt % RuO_2) at different constant current discharge values.

the solid particle becomes a dominant limiting factor. Therefore, this dimensionless parameter allows one to examine the relationship between the particle size and the discharge rate quickly.

Where *Sc* is small, mass-transfer limitations in the electrolyte can affect the performance of the electrode. We study this by looking at the galvanostatic discharge behavior of the cell with different oxide particle sizes.

Figure 8 shows the galvanostatic discharge curves of the RuO_2/carbon composite (60 wt % RuO_2). The porosity and particle size of the oxide were fixed at 0.181 and 50 nm, respectively. The charge delivered decreases as the discharge cell current density increases. The resulting decrease can be attributed to the concentration polarization within the pores caused by transport limitations if the diffusion in the oxide particle remains the same. To prove this, the salt concentration distributions at the end of the galvanostatic discharge are obtained over the cell thickness and are shown in Fig. 9. The initial concentration of the electrolyte is taken as 1 M. As discharge proceeds, the salt concentration increases in the negative electrode and decreases symmetrically in the positive electrode. As shown in Eq. 1 during discharge H^+ ions are consumed at the positive electrode and are produced at the negative electrode. The net reaction is one of transport of protons from the negative to the positive electrode. Ideally, the total electrolyte concentration is conserved. However, as shown in Fig. 9 significant variations are seen across the cell. Increasing cell current density causes significant depletion of electrolyte in the positive electrode due to consumption in the faradaic reaction. This in turn leads to an increase in the concentration polarization due to mass-transfer limitations in the bulk electrolyte.

To examine how concentration polarization has an effect on the cell performance, the solution potential drop inside the electrode is shown in Fig. 10. As expected, the solution potential drops sharply

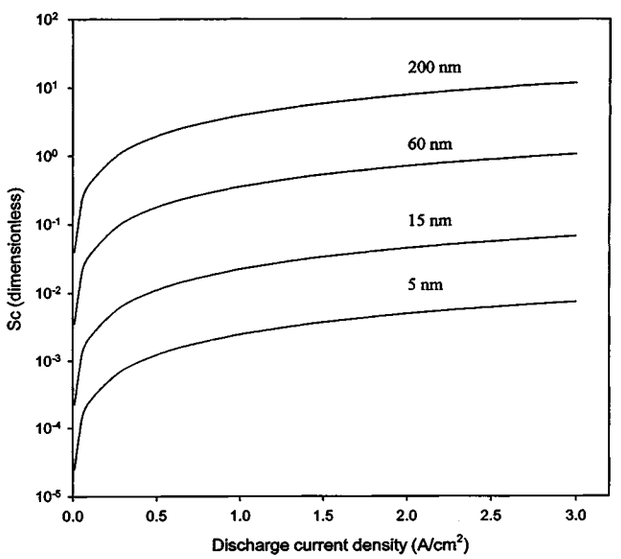

Figure 7. Dimensionless parameter, *Sc* (diffusion in the solid/discharge time), as a function of particle size of RuO_2. RuO_2: 40 wt %, porosity: 0.214, C_t: 0.015 mol/cm^3.

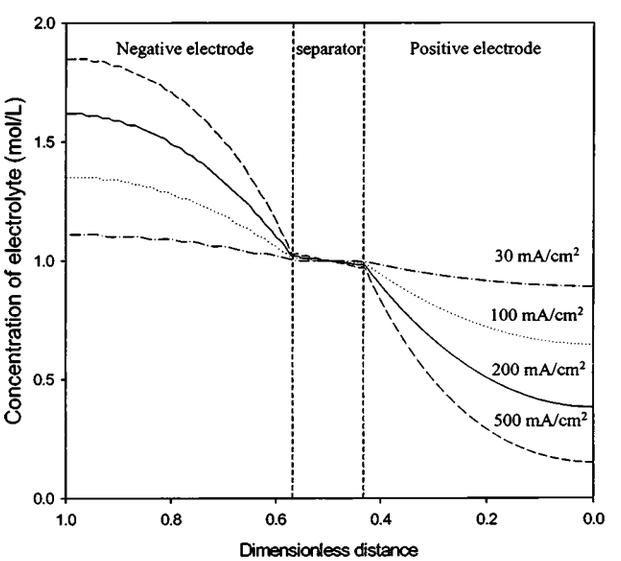

Figure 9. Electrolyte concentration distribution of the cell at the end of discharge with different current densities. RuO_2: 60 wt %, porosity: 0.181, particle size: 50 nm.

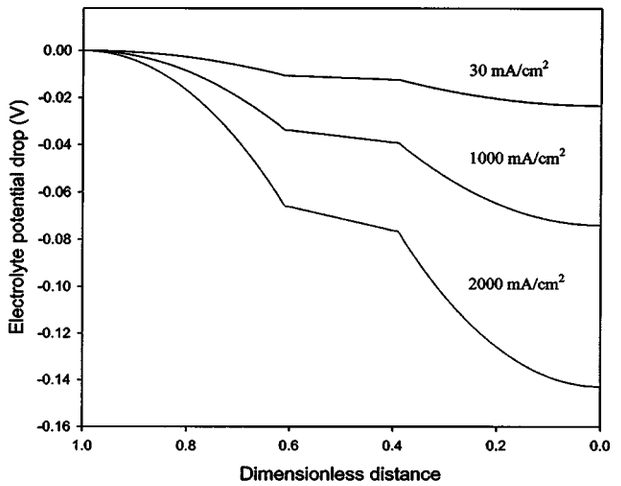

Figure 10. Potential distribution in the electrolyte at the end of discharge with different current densities.

with increasing discharge current density. The significant depletion of electrolyte that develops in the porous electrode phase is another dominant factor for limiting the capacitor performance at high discharge rates.

To reduce potential drop in the solution phase, increase in electrode porosity has been suggested.[18] A porosity of 1 corresponds to a fully flooded electrolyte. Figure 11 illustrates the potential drop in the solution phase while changing the porosity of the electrode. The discharge current density is 1 A/cm^2 and the rest of the parameters are the same as in Fig. 8. According to this graph, the drop in solution potential becomes less pronounced when the porosity of the electrode increases. Increasing the porosity has the simple effect of making the electrolyte more accessible to all the pores within the electrode thereby leading to a decrease in the concentration polarization in the cell.

Figure 12 demonstrates how this model can be used to optimize the composition of the electrode at discharge rate of 1.5 A/cm^2 when different particle sizes of RuO_2 and carbon are physically mixed. For the same content of RuO_2 (60 wt %) in the composite mixture,

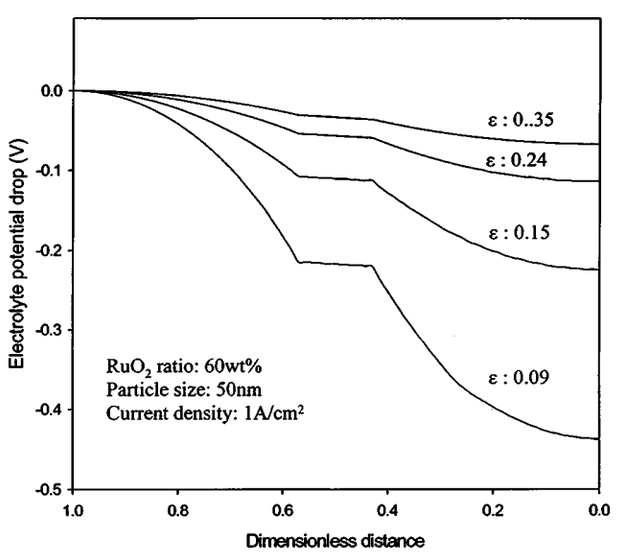

Figure 11. Potential distribution in the electrolyte at the end of discharge for different electrode porosities.

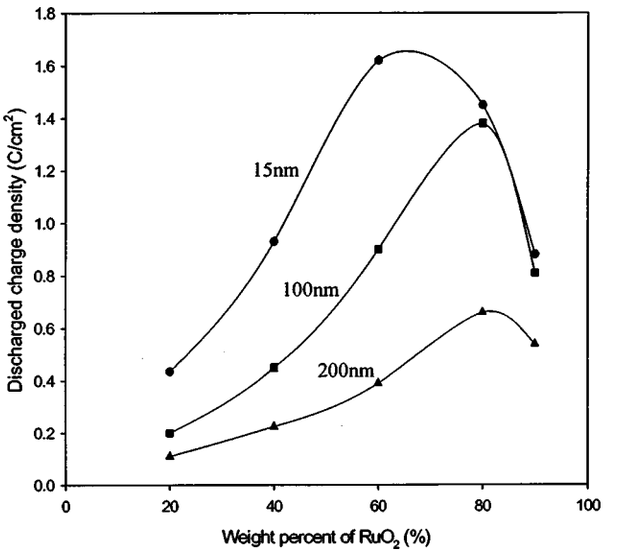

Figure 12. Discharged charge density as a function of RuO_2 content and particle size of RuO_2 at the constant discharge rate of 1.5 A/cm^2. The concentration of electrolyte is 1 M.

the smaller particle size of RuO_2 shows higher discharge density. As discussed above, these phenomena are associated with the effect of diffusion of the proton in the particle. As shown in Fig. 12, the charge density increases almost linearly with increase of the weight percentage of RuO_2 in the composite mixture, goes through a maximum, and then starts to decrease with further increase in the RuO_2 content. The observed decrease in the charge density is due to the concentration polarization in the electrolyte. The maximum is observed for lower concentrations of RuO_2 in the composite mixture as the particle size of RuO_2 decreases. In small particles, the surface area in contact with electrolyte is large resulting in an increase of the amount of electrolyte required for the reaction. To improve the transportation of the electrolyte, it is necessary to increase the porosity of electrode, which can be accomplished by increasing the carbon content in the electrode.

The other critical factor for higher performance of the active material is the initial concentration of the electrolyte. In Fig. 13, the particle size of RuO_2 and the discharge current density are fixed at 15 nm and 1.5 A/cm^2, respectively. With increasing concentration of the electrolyte from 1 to 3 M, the content of RuO_2 can be increased up to 85 wt % without sacrificing the performance. The maximum discharge density also increases from 1.86 to 2.8 C/cm^2. High initial concentration of the electrolyte compensates for the polarization of electrolyte caused by slow transportation. The model results indicated that the performance of the active material depends on the type of the carbon, the particle size of oxide, the concentration of electrolyte, and the peak discharge current.

Figure 14 shows Ragone plots of RuO_2/carbon composite electrodes prepared by a deposition process such as a colloidal method.[19] Each electrode has a different porosity, particle size, and RuO_2 content. This simulation result shows that RuO_2 alone cannot be used as capacitor electrodes due to its poor rate capability resulting from the low porosity and the large particle size. This is in accordance with previous experimental data.[18,19] In reality, the porosity of the electrode varies even at the same carbon/RuO_2 ratio according to the particle size of RuO_2 and also in the way RuO_2 and carbon are mixed (physical or chemical mixture). It has been shown that large particles of RuO_2 deposited chemically block the pores of the carbon, which cannot be expected to reduce the solution potential drop.[19] For example, 60 wt % of carbon produces a porosity of 0.181 in a physical mixture while the chemical mixture has

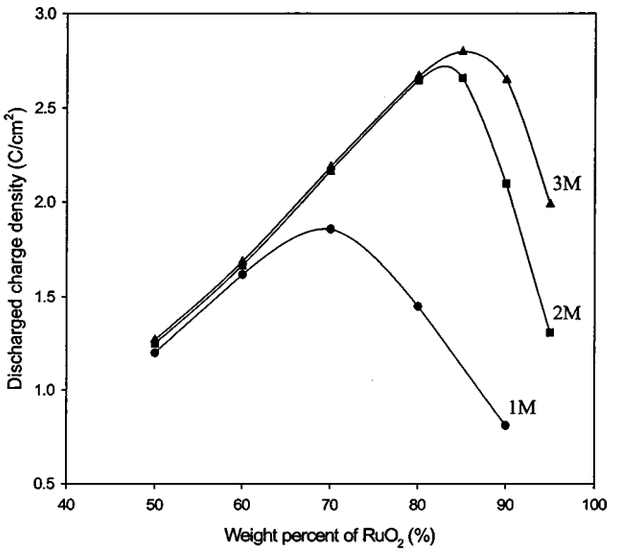

Figure 13. Discharged charge density as a function of RuO_2 content and concentration of electrolyte at the constant discharge rate of 1.5 A/cm^2. Particle size of RuO_2 is 15 nm.

0.124 at the same carbon ratio. When the ratio of RuO_2 is 40 wt %, nanosize of particles and high porosity are achieved, generating the highest energy density at 5 kW/kg of power load. This data suggests that decreasing the particle size and increasing the porosity of the electrode can reduce the cost of the supercapacitor.

Conclusions

A general model is developed for supercapacitors containing two identical oxide/carbon composite electrodes and separator when diffusion takes place in oxides. Simulation results are presented for the typical RuO_2/carbon system. This model is used to investigate the effect of porosity and particle size of oxide at different discharge rates. The particle size of oxide is still a critical factor in determining the performance especially at high discharge rates because diffusion in the oxide is the limiting step. With increasing electrode porosity, the drop in solution potential reduces and the rate capability increases. The optimum porosity of the electrode can be calculated for given conditions and the corresponding carbon ratio can also be obtained using the present model. Also, this model allows us to evaluate the performance of the cell at different operating conditions and suggests guidelines for optimization of the system.

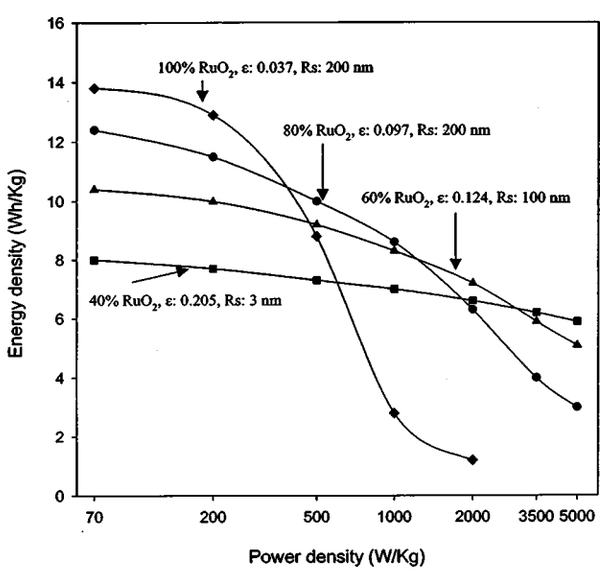

Figure 14. Ragone plot for RuO_2/carbon composite electrodes containing different Ru loading prepared by a colloidal method.

Acknowledgments

The authors are grateful for the financial support by the Commission on Higher Education Fund no. 15510-G112 and the National Reconnaissance Organization (NRO) under contract no. NRO-00-C-0134.

University of South Carolina assisted in meeting the publication costs of this article.

List of Symbols

A_c	specific surface area of carbon, m^2/g
C	electrolyte concentration, mol/cm^3
C^0	initial concentration of electrolyte, mol/cm^3
C_s	concentration of proton in the RuO_2, mol/cm^3
C_t	maximum concentration of proton in RuO_2, mol/cm^3
C_0	solvent concentration, mol/cm^3
D	effective diffusion coefficient of electrolyte, cm^2/s
D_0	diffusion coefficient of electrolyte in the bulk solution, cm^2/s
D_s	diffusion coefficient of proton in the oxide, cm^2/s
d_{RuO_2}	particle diameter of RuO_2
F	Faraday's constant, 96,484 C/equiv
$f_{\pm}$	electrolyte activity coefficient
i_0	exchange current density of faradaic reaction, A/cm^2
i_1	superficial current density in the solid phase, A/cm^2
i_2	superficial current density in the solution phase, A/cm^2
I	cell current density, A/cm^2
j_f	faradaic transfer current density for the RuO_2 reaction, A/cm^2
k_p	effective ionic conductivity of electrolyte, S/cm
k_{p0}	ionic conductivity of electrolyte in the bulk solution, S/cm
L_e	thickness of electrode, cm
L_s	thickness of separator, cm
M_{RuO_2}	molecular weight of RuO_2
n	number of electrons transferred in the electrode reaction
P_d	double-layer capacitance per area of electrode, F/cm^2
R	universal gas constant, 8.314 J/mol K
R_s	radius of RuO_2 particle, cm
r	distance normal to surface of RuO_2 particle, cm
S_d	specific surface area for double-layer capacitance per unit electrode volume, cm^2/cm^3
S_f	specific surface area for pseudocapacitance per unit electrode volume, cm^2/cm^3
s^+	stoichiometric coefficient of cations in electrode reaction
T	temperature, K
t	time, s
t_+^0	cation transference number
U_1	equilibrium potential for the faradaic reaction, V
V_0	initial equilibrium potential, V
v_c	volume fraction of carbon
v_{RuO_2}	volume fraction of RuO_2
z^+	charge number
Greek	
α_a	anodic transfer coefficient of the faradaic reaction
α_c	cathodic transfer coefficient of the faradaic reaction
ε	porosity of electrode
ε_s	porosity of separator
v^+	number of cations into which a mole of electrolyte salt dissociates
ρ_c	density of carbon, g/cm^3
ρ_{ox}	density of RuO_2, g/cm^3
σ	electronic conductivity in the solid phase, S/cm
Φ_1	solid phase potential, V
Φ_2	solution phase potential, V

References

1. F. A. Posey and T. Morozumi, *J. Electrochem. Soc.*, **113**, 176 (1966).
2. A. M. Johnson and J. Newman, *J. Electrochem. Soc.*, **118**, 510 (1971).
3. B. Pillay and J. Newman, *J. Electrochem. Soc.*, **143**, 1806 (1996).
4. V. Srinivasan and J. W. Weidner, *J. Electrochem. Soc.*, **146**, 1650 (1999).
5. C. J. Farahmandi, in *Electrochemical Capacitors II*, F. M. Delnick, D. Ingersoll, X. Andrieu, and K. Naoi, Editors, PV 96-25, p. 167, The Electrochemical Society Proceedings Series, Pennington, NJ (1996).

6. C. Lin, J. A. Ritter, B. N. Popov, and R. E. White, *J. Electrochem. Soc.*, **146**, 3168 (1999).
7. C. Lin, B. N. Popov, and H. J. Ploehn, *J. Electrochem. Soc.*, **149**, A167 (2002).
8. J. P. Zheng and T. R. Jow, *J. Electrochem. Soc.*, **142**, L6 (1995).
9. J. P. Zheng, P. J. Cygan, and T. R. Jow, *J. Electrochem. Soc.*, **142**, 2699 (1995).
10. M. Doyle, T. F. Fuller, and J. Newman, *J. Electrochem. Soc.*, **140**, 1526 (1993).
11. T. R. Jow and J. P. Zheng, *J. Electrochem. Soc.*, **145**, 49 (1998).
12. T. Liu, W. G. Pell, and B. E. Conway, *Electrochim. Acta*, **42**, 3541 (1997).
13. J. Newman, *Electrochemical Systems*, 2nd ed., Prentice-Hall, Englewood Cliffs, NJ (1991).
14. J. Newman and W. Tiedemann, *AIChE J.*, **21**, 25 (1975).
15. B. Leimkuhler, L. R. Petzold, and C. W. Gear, *SIAM (Soc. Ind. Appl. Math.) J. Numer. Anal.*, **28**, 205 (1991).
16. G. S. Nagarajan, J. W. Van Zee, and R. M. Spotnitz, *J. Electrochem. Soc.*, **145**, 771 (1998).
17. A. B. Yu, R. P. Zou, and N. Standish, *Ind. Eng. Chem. Res.*, **35**, 3730 (1996).
18. J. P. Zheng, *Electrochem. Solid-State Lett.*, **2**, 359 (1999).
19. H. Kim and B. N. Popov, *J. Power Sources*, **104**, 52 (2002).
20. J. M. Miller and B. Dunn, *J. Electrochem. Soc.*, **144**, L309 (1997).
21. W. C. Shin and S. G. Yoon, *J. Electrochem. Soc.*, **144**, 1055 (1997).
22. K. Kinoshita, *Carbon: Electrochemical and Physicochemical Properties*, John Wiley & Sons, New York (1988).
23. J. P. Zheng and T. R. Jow, U.S. Pat. 5,961,887 (1999).
24. V. M. M. Lobo, *Electrolyte Solutions: Literature Data on Thermodynamic and Transport Properties*, Coimbra, Publ. Co., Coimbra, Portugal (1975).